Aerospace Science and Technology 105 (2020) 106030

Contents lists available at ScienceDirect

Aerospace Science and Technology

www.elsevier.com/locate/aescte

Model-based path prediction for fixed-wing unmanned aircraft using pose estimates

Changkoo Kang [1], Craig A. Woolsey [*,2]

Department of Aerospace and Ocean Engineering, Virginia Tech, Blacksburg, VA 24061, USA

ARTICLE INFO

Article history:
Received 31 December 2019
Received in revised form 11 March 2020
Accepted 12 June 2020
Available online 25 June 2020
Communicated by Amit Kumar Sanyal

Keywords:
Unmanned aircraft
Flight mechanics
Path prediction
Computer vision

ABSTRACT

With the rapid proliferation of small unmanned aircraft systems (sUAS), there is an increasing need for these aircraft to detect and predict each other's motion in order to avoid collisions. This concern arises in addition to the well-established need to detect and avoid manned aircraft. The two threats pose distinct challenges. For example, while a manned aircraft typically travels quite fast compared with a sUAS, its path can be accurately predicted over moderate time intervals using only position measurements and a kinematic particle model. Because sUAS are more maneuverable, and detection horizons can be much shorter, there is a need for more sophisticated prediction methods. One way to improve accuracy is to base predictions on the complete pose (position and attitude) and a higher fidelity model of the threat aircraft's dynamics. As an initial demonstration, we propose an algorithm to predict the path of a small, fixed-wing unmanned aircraft using estimates of this threat aircraft's pose, as might be obtained using visual sensors. To assess the algorithm's performance, predictions using the proposed algorithm are compared with predictions based solely on position data for a large experimental data set. The results indicate that the proposed algorithm outperforms the position-only prediction method.

1. Introduction

As the personal and professional uses of small unmanned aircraft systems (sUAS) continue to expand, and the number of these aircraft increases, concern is rising about the possibility of malicious mis-use and mid-air collisions. Concern about collisions between sUAS and manned aircraft is supported by recent unauthorized flights of sUAS over major airports that have resulted in airport closures and travel disruptions [1]. Long before concerns about sUAS arose, however, the aviation industry was addressing the risk of mid-air collisions between manned aircraft.

Conflict detection and resolution (CD&R) technologies, such as the traffic alert and collision avoidance system (TCAS), have played an important role in air traffic management (ATM) since at least the early 1990s [2,3]. CD&R technologies for manned aircraft are supported by a large amount of aircraft performance model (APM) data, which has enabled extensive research and development of path prediction methods for manned aircraft. Recent emphasis on direct, real-time flight data transfer among aircraft has enabled even more accurate path prediction using flight safety communication systems such as automatic dependent surveillance-broadcast (ADS-B) [4,5].

With the proliferation of sUAS, and the recognition that these aircraft operate very differently than manned aircraft, there has also been recent interest in developing path prediction methods for this class of aircraft. Many of the CD&R studies for sUAS focus on path prediction using only position data. In these studies, the sUAS is typically assumed as a particle, and the velocity and acceleration are computed as the first and second time derivatives of position, respectively. The future position of the sUAS is then propagated with time [6,7]. In references [8], [9] and [10], the path is predicted under the simplifying assumption that the threat moves with constant velocity or with constant acceleration. Based on a similar particle dynamic model, references [11] and [12] predict the flight path using a Kalman filter, while references [13] and [14] instead use a particle filter. Reference [15] defines the reachable set of the sUAS in order to ensure collision avoidance. Small unmanned aircraft have the ability to maneuver much more aggressively than manned aircraft, however, and they are more susceptible to wind disturbances, so path prediction methods that are based solely on the position history of the threat aircraft may not provide sufficient warning to inform a CD&R system. These prediction methods assume a particle dynamic ("aircraft performance") model for the threat aircraft, but accurate performance models may be unavailable [16].

* Corresponding author.
E-mail addresses: changkk@vt.edu (C. Kang), cwoolsey@vt.edu (C.A. Woolsey).
[1] Graduate Research Assistant, Department of Aerospace and Ocean Engineering.
[2] Professor, Department of Aerospace and Ocean Engineering.

https://doi.org/10.1016/j.ast.2020.106030
1270-9638/

In considering path prediction for sUAS, it is helpful to review methods that have been proposed for manned aircraft. ATM-related path prediction methods normally assume known flight data, such as thrust, mass, position and other variables associated with point mass models (PMMs) [17–22]. Recent work concerning aircraft path prediction used radar and weather data from ground-based systems to infer the path, as in [23–27]. For model-based path prediction, it can be helpful to know, or to estimate, the mass or thrust of the threat aircraft. Alligier et al. [28] suggested a prediction algorithm based on an estimate of the mass of the threat aircraft developed using energy rate and learning algorithms. Thipphavong et al. [29] also estimated the mass of the threat aircraft to inform the path prediction. In [30] and [31], the aircraft thrust was estimated. These studies used mature manned aircraft performance models, such as the Base of Aircraft Data (BADA) model of EUROCONTROL [32], but such models may be inappropriate or impractical for a maneuvering sUAS.

We propose a path prediction method that uses an estimate of the pose of a threat aircraft, focusing on fixed-wing airplanes. The idea that a threat aircraft's pose may be available to inform path prediction is supported by the increasing sophistication of computer vision based sensing systems, as mentioned above. With the development of lightweight, low-power camera technologies, a host aircraft can easily acquire high resolution images from which the attitude of a threat aircraft can be obtained using computer vision and machine learning [33–39]. Active sensing, such as radar, has shown good performance for position estimation of threat sUAS [40–43]. Therefore, the position and attitude of a threat sUAS can be extracted from an on-board sUAS sensing system of a host aircraft. We propose a new model-based path prediction algorithm for a small, fixed-wing, unmanned aircraft which incorporates an estimate of the threat's attitude, as well as its position.

We first introduce an algorithm to estimate two types of specific power of a threat aircraft, the conventional specific excess power and an energy-conserving specific power that accounts for changes in path direction. These power terms are inferred from position and attitude data obtained from visual imagery, for example, and are then used in a particle dynamic model of the threat aircraft's motion for path prediction. The proposed prediction algorithm and an amended algorithm which also estimates wind velocity are compared with a more conventional position-based prediction method.

The paper is organized as follows. Section 2 describes the proposed path prediction algorithms. Section 3 describes the unmanned aircraft, and associated flight data, which are used to test and evaluate the algorithm. Section 4 details the main results. Concluding remarks and a brief description of ongoing work are presented in Section 5.

2. Path prediction algorithm

Consider a fixed-wing unmanned aircraft modeled as a point mass and let $\vec{\boldsymbol{r}} = [x, y, z]^T$ denote the position of the threat aircraft in a global frame, which is assumed to be an inertial reference frame. The position variables are assumed to be extracted from an on-board sUAS sensing system. Also define the inertial velocity $\vec{\boldsymbol{v}} = [\dot{x}, \dot{y}, \dot{z}]^T$ and acceleration $\vec{\boldsymbol{a}} = [\ddot{x}, \ddot{y}, \ddot{z}]^T$. Finally, define the vector

$$\boldsymbol{X} = [\vec{\boldsymbol{r}}^T, \vec{\boldsymbol{v}}^T, \vec{\boldsymbol{a}}^T]^T \tag{1}$$

by concatenating position, velocity, and acceleration. For a small, constant, discrete time step Δt, the aircraft position, velocity, and acceleration at time t_{k+1} can be estimated from the values at time t_k as follows:

$$\boldsymbol{X}_{k+1} = \begin{bmatrix} I_{3\times3} & \Delta t & \frac{1}{2}(\Delta t)^2 \\ 0 & I_{3\times3} & \Delta t \\ 0 & 0 & I_{3\times3} \end{bmatrix} \boldsymbol{X}_k \tag{2}$$

Because the position history obtained from measurements is likely to be noisy, the velocity at time-step k may be estimated using a moving window average of finite differences over the past n time steps

$$\vec{\boldsymbol{v}}_k = \frac{1}{n\Delta t} \sum_{i=k-n+1}^{k} (\vec{\boldsymbol{r}}_i - \vec{\boldsymbol{r}}_{i-1}) \tag{3}$$

where $\vec{\boldsymbol{r}}_i$ is the position estimate of the threat aircraft at time step i. For the acceleration, two estimation approaches are considered: (1) using a moving window average of finite differences, as above, and (2) using a particle dynamic model for aircraft motion. The first approach is often used since it requires no model and performs well when the threat aircraft is operating near steady state [44]. However, a sUAS is maneuverable and susceptible to wind disturbances, so its acceleration can change quickly. The second approach uses the position and attitude data, together with aircraft equations of motion, to estimate the aircraft acceleration. This approach responds more quickly to changes in acceleration than the first method. The latter approach was considered in [33] for 2D flight and was shown to perform better than the first method for predicting steady turning flight paths. In this paper, the two approaches are compared for more general cases of 3D flight.

Using the second approach, the acceleration $\vec{\boldsymbol{a}}$ can be computed using the threat aircraft velocity and its orientation, with the understanding that the aircraft's attitude influences the aerodynamic forces affecting its motion. Let $\boldsymbol{\Omega} = [0, \dot{\gamma}, \dot{\psi}\cos\gamma]^T$ where γ and ψ are the flight path angle and course angle, respectively. These angles are extracted from the threat's inertial velocity, which is inferred from measurements by the host aircraft. The algorithm to compute the angular rates is described shortly. The acceleration $\vec{\boldsymbol{a}}$ is

$$\begin{aligned} \vec{\boldsymbol{a}} &= \vec{\boldsymbol{a}}_{\mathrm{t}} + \vec{\boldsymbol{a}}_{\mathrm{n}} \\ &= \vec{\boldsymbol{a}}_{\mathrm{t}} + \boldsymbol{\Omega} \times \vec{\boldsymbol{v}} \end{aligned} \tag{4}$$

where $\vec{\boldsymbol{a}}_{\mathrm{t}}$ is the acceleration tangent to the flight path and $\vec{\boldsymbol{a}}_{\mathrm{n}}$ is the acceleration normal to the flight path. Each acceleration vector can be computed using the particle dynamic equations of motion for a fixed wing aircraft:

$$\frac{dx}{dt} = V\cos\gamma\cos\psi \tag{5}$$

$$\frac{dy}{dt} = V\cos\gamma\sin\psi \tag{6}$$

$$\frac{dz}{dt} = V\sin\gamma \tag{7}$$

$$\frac{dV}{dt} = g\left(\frac{T-D}{W} - \sin\gamma\right) \tag{8}$$

$$\frac{d\gamma}{dt} = \frac{g}{V}\left(\frac{L}{W}\cos\phi - \cos\gamma\right) \tag{9}$$

$$\frac{d\psi}{dt} = \frac{g}{V}\frac{L}{W}\frac{\sin\phi}{\cos\gamma} \tag{10}$$

where L, W, T and D are lift, weight, thrust and drag force, respectively, ϕ is the roll angle of the aircraft, $V = \|\vec{v}\|$ is airspeed, assuming flight in still air, and g is the local specific force of gravity. Using these equations, $\boldsymbol{\Omega}$ and $\vec{\boldsymbol{v}}$ in (4) are estimated under the

assumption that lift is perpendicular to thrust which, in turn, is aligned with the flight path [45,46].

2.1. Acceleration in steady flight

In order to compute acceleration using (8)-(10), the unknown forces L, W, T and D are required. In this subsection, we make the simplifying assumption that the threat aircraft is always in a state of steady flight, the most general case of which is constant-speed flight at a constant climb angle and a constant turn rate, i.e., constant-speed flight along a vertical helix. Noting that V and γ are constant in steady flight, equations (8)-(9) imply that [44,47–49]:

$$T = W\sin\gamma + D \tag{11}$$

$$L\cos\phi = W\cos\gamma \tag{12}$$

Equation (10) then gives

$$\dot{\psi} = \frac{g}{V}\tan\phi \tag{13}$$

Since $\vec{\boldsymbol{a}}_{\mathrm{t}}$ and $\dot{\gamma}$ are zero in steady flight,

$$\vec{\boldsymbol{a}} = \boldsymbol{\Omega}\times\vec{\boldsymbol{v}} = \begin{bmatrix} 0 \\ 0 \\ \dot{\psi}\cos\gamma \end{bmatrix} \times \begin{bmatrix} \dot{x} \\ \dot{y} \\ \dot{z} \end{bmatrix} = \begin{bmatrix} -\frac{g}{V}\dot{y}\tan\phi\cos\gamma \\ \frac{g}{V}\dot{x}\tan\phi\cos\gamma \\ 0 \end{bmatrix} \tag{14}$$

2.2. Estimation of acceleration in unsteady flight

The equations in the previous section work well for wings-level or steady, turning flight. However, sUAS can change their acceleration quickly, due either to control inputs or to disturbances. In these cases, the steady flight assumption is inappropriate. Here, the steady flight assumption is relaxed and the acceleration is estimated using concepts of specific energy and power. First, because the speed of the aircraft may change, $\vec{\boldsymbol{a}}_{\mathrm{t}}$ in (4) is no longer zero:

$$\begin{aligned}\vec{\boldsymbol{a}} = \vec{\boldsymbol{a}}_{\mathrm{t}} + \boldsymbol{\Omega}\times\vec{\boldsymbol{v}} &= \begin{bmatrix} \ddot{x}_t \\ \ddot{y}_t \\ \ddot{z}_t \end{bmatrix} + \begin{bmatrix} 0 \\ \dot{\gamma} \\ \dot{\psi}\cos\gamma \end{bmatrix} \times \begin{bmatrix} \dot{x} \\ \dot{y} \\ \dot{z} \end{bmatrix} \\ &= \begin{bmatrix} \ddot{x}_t - \dot{\psi}\,\dot{y}\cos\gamma + \dot{\gamma}\,\dot{z} \\ \ddot{y}_t + \dot{\psi}\,\dot{x}\cos\gamma \\ \ddot{z}_t - \dot{\gamma}\,\dot{x} \end{bmatrix}\end{aligned} \tag{15}$$

In this case, the forces no longer balance as in (11) and (12).

The applied forces needed to estimate the acceleration of the threat aircraft are unknown. Here, the energy rate of the aircraft is estimated in order to approximate these forces. Reformulating equation (8) in terms of specific excess power gives [29,50–52]:

$$\frac{(T-D)V}{m} = V\dot{V} + g\dot{z} \tag{16}$$

The left-hand side of (16) is the specific excess power and the right-hand side is the rate of change of specific energy due to (i) along-track acceleration and (ii) climbing in a gravitational field.

Similarly, equation (9) is reformulated as

$$\frac{LV}{m} = \frac{V}{\cos\phi}\left(V\dot{\gamma} + g\cos\gamma\right) \tag{17}$$

Like (16), the left-hand side of (17) has units of specific power. This power is due to lift, however, rather than excess thrust. It accounts for energy-conserving changes in the flight path direction.

Alligier et al. [50,51] proposed least squares estimation of the aircraft mass based on the path history for climb path prediction. In their work, T and D are known, allowing one to compute the mass from (16). For the case considered in this paper, T, D and m are all unknown, so the specific excess power

$$P_{\mathrm{excess}} = \frac{(T-D)V}{m} \tag{18}$$

is estimated instead of the mass. Equation (16) enables one to estimate P_{excess} by computing the specific energy rate $\dot{E}_{\mathrm{excess}} = V\dot{V} + g\dot{z}$ of a data point:

$$P_{\mathrm{excess}} = \dot{E}_{\mathrm{excess}} \tag{19}$$

Here, the along-track acceleration $\dot{V}$ is estimated from measurements using a moving window average, as in (3). A least-squares estimate based on several consecutive data points is used. In this formulation, P_{excess} is assumed to remain constant over a short time window (e.g., 1 second). Computing the cumulative squared error between the estimated constant value of P_{excess} and the computed values $\dot{E}_{\mathrm{excess}}$ over n data points up to time step k gives

$$e_{\mathrm{excess}_k} = \frac{1}{n}\sum_{i=k-n+1}^{k}\left(P_{\mathrm{excess}} - \dot{E}_{\mathrm{excess}_i}\right)^2 \tag{20}$$

The best estimate of P_{excess} is the least square solution obtained by solving

$$\frac{de_{\mathrm{excess}_k}}{dP_{\mathrm{excess}}} = 0 \qquad \Rightarrow \qquad P_{\mathrm{excess}_k} = \frac{1}{n}\sum_{i=k-n+1}^{k}\dot{E}_{\mathrm{excess}_i} \tag{21}$$

That is, P_{excess_k} is taken as the average specific energy rate over n previous time steps.

In a similar way, referring to (17), the specific power acting normal to the flight path is

$$P_{\mathrm{norm}} = \frac{LV}{m} \tag{22}$$

This term may be computed in terms of the energy rate

$$\dot{E}_{\mathrm{norm}} = \frac{V}{\cos\phi}\left(V\dot{\gamma} + g\cos\gamma\right) \tag{23}$$

As before, P_{norm} is assumed to remain constant over an n-step time horizon yielding the approximation

$$P_{\mathrm{norm}_k} = \frac{1}{n}\sum_{i=k-n+1}^{k}\dot{E}_{\mathrm{norm}_i} \tag{24}$$

The resulting specific power terms, P_{excess} and P_{norm}, are substituted directly into the aircraft equations of motion (8)-(10) noting that

$$\frac{T-D}{W} = \frac{P_{\mathrm{excess}}}{Vg} \tag{25}$$

$$\frac{L}{W} = \frac{P_{\mathrm{norm}}}{Vg} \tag{26}$$

Thus, we have

$$\frac{dV}{dt} = \left(\frac{P_{\mathrm{excess}}}{V} - g\sin\gamma\right) \tag{27}$$

$$\frac{d\gamma}{dt} = \frac{1}{V}\left(\frac{P_{\mathrm{norm}}}{V}\cos\phi - g\cos\gamma\right) \tag{28}$$

$$\frac{d\psi}{dt} = \frac{P_{\mathrm{norm}}}{V^2}\frac{\sin\phi}{\cos\gamma} \tag{29}$$

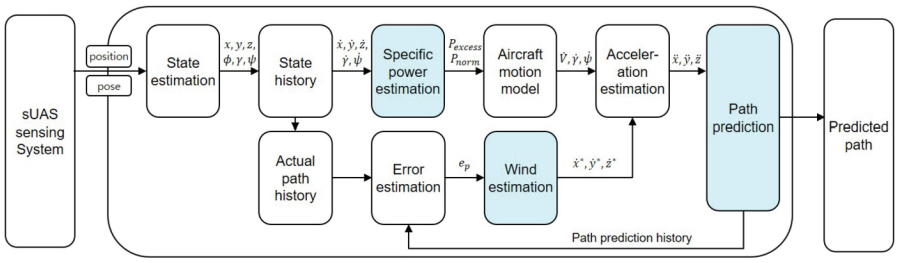

Fig. 1. Flow chart of the algorithm.

The acceleration in (27) is projected onto each axis to determine the components of tangential acceleration:

$$\begin{aligned}\ddot{x}_t &= \left(\frac{P_{\text{excess}}}{V} - g\sin\gamma\right)\cos\gamma\cos\psi \\ \ddot{y}_t &= \left(\frac{P_{\text{excess}}}{V} - g\sin\gamma\right)\cos\gamma\sin\psi \\ \ddot{z}_t &= \left(\frac{P_{\text{excess}}}{V} - g\sin\gamma\right)\sin\gamma\end{aligned} \tag{30}$$

In the end, one obtains the following expressions for acceleration of the threat aircraft:

$$\vec{\boldsymbol{a}} = \begin{bmatrix} \left(\frac{P_{\text{excess}}}{V} - g\sin\gamma\right)\cos\gamma\cos\psi - \frac{P_{\text{norm}}}{V^2}\dot{y}\sin\phi + \frac{1}{V}\left(\frac{P_{\text{norm}}}{V}\cos\phi - g\cos\gamma\right)\dot{z} \\ \left(\frac{P_{\text{excess}}}{V} - g\sin\gamma\right)\cos\gamma\sin\psi + \frac{P_{\text{norm}}}{V^2}\dot{x}\sin\phi \\ \left(\frac{P_{\text{excess}}}{V} - g\sin\gamma\right)\sin\gamma - \frac{1}{V}\left(\frac{P_{\text{norm}}}{V}\cos\phi - g\cos\gamma\right)\dot{x} \end{bmatrix} \tag{31}$$

Finally, the resulting velocity and acceleration are concatenated to form the state vector $\boldsymbol{X}_k$ and the future path of the threat is estimated as in (2).

2.3. Correcting for wind

To estimate and correct for the wind, we compare the predicted path with the measured path, attributing any error to wind disturbances. More specifically, we formulate an optimization problem to determine the aircraft velocity that minimizes path prediction error. The difference between this minimum-error velocity and the velocity predicted as described above provides an estimate of the ambient wind.

Given the current position $\vec{\boldsymbol{r}}_k$, velocity $\vec{\boldsymbol{v}}_k$ from (3), and acceleration $\vec{\boldsymbol{a}}_k$ from (31), the position l time steps in the future can be estimated using (2):

$$\vec{\boldsymbol{r}}^{\,\text{p}}_{k+l} = \vec{\boldsymbol{r}}_k + \vec{\boldsymbol{v}}_k(l\Delta t) + \frac{1}{2}\vec{\boldsymbol{a}}_k(l\Delta t)^2 \tag{32}$$

$$= \vec{\boldsymbol{r}}_k + \vec{\boldsymbol{v}}_k(l\Delta t) + \frac{1}{2}\left(\vec{\boldsymbol{a}}_{\text{t}_k} + \boldsymbol{\Omega}_k \times \vec{\boldsymbol{v}}_k\right)(l\Delta t)^2 \tag{33}$$

In order to compare the actual position history and the predicted position history, an averaged distance error at time step k between the two n-step histories is estimated as follows:

$$e^{\text{p}}_k = \frac{1}{n}\sum_{i=k-n+1}^{k}\sqrt{\left\|\vec{\boldsymbol{r}}^{\,\text{a}}_i - \vec{\boldsymbol{r}}^{\,\text{p}}_i\right\|^2} \tag{34}$$

where $\vec{\boldsymbol{r}}^{\,\text{a}}_i$ is the actual position, and $\vec{\boldsymbol{r}}^{\,\text{p}}_i$ is the predicted position at time i. Having defined an error metric, we may seek a velocity value $\vec{\boldsymbol{v}}^{\,*}_k$ which minimizes the error e^{p}_k. This optimal velocity is obtained by solving the following equations:

$$\vec{\boldsymbol{v}}^{\,*}_k = \arg\min_{\vec{\boldsymbol{v}}_k} e^{\text{p}}_k = \arg\min_{\vec{\boldsymbol{v}}_k}\frac{1}{n}\sum_{i=k-n+1}^{k}\sqrt{\left\|\vec{\boldsymbol{r}}^{\,\text{a}}_i - \vec{\boldsymbol{r}}^{\,\text{p}}_i\right\|^2} \tag{35}$$

The difference between the minimum-error velocity $\vec{\boldsymbol{v}}^{\,*}_k$ obtained through the optimization process above and the estimate $\vec{\boldsymbol{v}}_k$ obtained by assuming flight through still air provides an estimate for the wind velocity:

$$\delta\vec{\boldsymbol{v}}_k = \vec{\boldsymbol{v}}^{\,*}_k - \vec{\boldsymbol{v}}_k \tag{36}$$

Note that this wind disturbance is based on a moving-window average; implicitly, the wind is assumed to vary slowly, in time and space, relative to this moving window. The algorithm described in this section is summarized in Fig. 1. In the following section, we compare prediction performance based on the optimized velocity $\vec{\boldsymbol{v}}^{\,*}_k$, which attempts to correct for the effect of wind, with the prediction performance using only position or position-plus-attitude measurements.

3. Flight data

In order to assess the proposed algorithm, experimental flight data for two fixed-wing sUAS, the eSPAARO and HobbyKing Bixler, are used. The publicly accessible Small Aircraft Flight Encounters (SAFE) Data Repository [53] includes flight data for these aircraft.

Each flight data set contains full state history data as well as estimates of wind speed. A flight of a fixed-wing sUAS generally consists of various, distinct segments including straight and level flight, turning flight, and maneuvering flight. In order to see how the path prediction performance differs for each type of flight, the flight data are parsed into these three types, as shown in Fig. 2.

Table 1 shows the number of each type of flight for each aircraft. As indicated in Table 2, the Bixler is lighter and smaller than the eSPAARO, so the Bixler is more maneuverable while the eSPAARO tends to fly more steadily. The Bixler has a greater number of maneuvering flight segments in the dataset than the eSPAARO. After segmenting the flight paths, three path prediction algorithms were applied to each type of flight path to compare the performance: (i) position-based prediction, (ii) pose-based prediction, and (iii) pose-plus-wind prediction. The position-based prediction algorithm estimates the acceleration by simply computing a discrete-time filtered derivative of velocity from telemetry data. The pose-based method uses the pose and aircraft equations of motion to estimate the acceleration as described in Section 2.2. For the purpose of this paper, pose is taken directly from the threat aircraft data log. In practice, pose would be inferred (with inevitable error) from visual imagery as suggested in [33]. The pose-plus-wind prediction algorithm computes the acceleration in the same way as the pose-based method and corrects the path

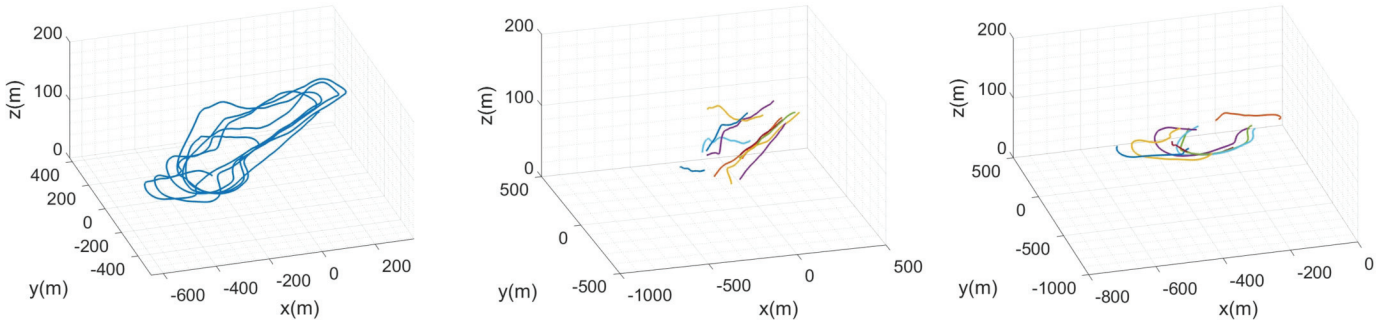

Fig. 2. Path segmentation for a representative flight test: Complete flight path history (left), straight flight segments (center), and turning flight segments (right).

Table 1
Number of paths used for algorithm evaluation.

Parameter	eSPAARO	Bixler
Straight flight	28	11
Turning flight	28	12
Maneuvering flight	7	20

Table 2
Specifications of aircraft used.

Parameter	eSPAARO	Bixler
Length	2.81 m	0.95 m
Wingspan	3.57 m	1.55 m
Mass	20 kg	1.2 kg
Propulsion power	740 W	28 W
Cruise speed	18 m/s	10 m/s

prediction as described in Section 2.3. The flight data includes the position and pose data of the aircraft with the GPS time. Using the GPS time, the algorithm is assessed by re-playing the flight data as shown in Fig. 3. This figure shows flight path data from a maneuvering flight of the Bixler aircraft. The light blue line depicts the actual path of the aircraft, and the red asterisk shows the aircraft position at the current time-step. The thick blue line indicates the predicted path, and the green line represents the actual path over the prediction time horizon (5 seconds). The following section describes a comparison of the three approaches to path prediction described earlier using flight test data.

4. Results

Path prediction performance for the two, small, fixed-wing unmanned aircraft described in Section 3 is evaluated by comparing the predicted path to the actual path of the aircraft. The left column of Fig. 3 shows an example of path prediction using the position-based approach, from two vantage points, and the right column shows the path prediction using the pose-plus-wind approach.

In the figure, the predicted path using the pose-plus-wind approach (right column, thick blue lines) is more similar to the actual path (green lines) over the prediction time horizon than the one using the position-based approach (left column, thick blue lines). Anecdotally, the pose-plus-wind prediction method performs at least as well – and sometimes significantly better – than the position-based method. Beyond the anecdotal evidence shown in Fig. 3, we present here a quantitative performance comparison for the flight segments identified in Table 1.

Although wind estimation is not the focus of this paper, the wind is a critical factor for sUAS path prediction. We therefore discuss some wind estimation results in this section, as well. Figs. 4 and 5 show the estimated wind disturbance and the actual wind velocity. (Here, the wind estimate provided by the threat aircraft's Pixhawk 1 autopilot is taken as the true wind velocity.) Red, blue and green lines indicate the three components of $\delta\vec{v}^* = [\delta v_x, \delta v_y, \delta v_z]^T$, respectively. Dashed red and blue lines show the true wind speed in the x direction (W_x) and the y direction (W_y), respectively. As can be seen in the figures, δv_x and W_x are comparable, as are δv_y and W_y, which indicates that the estimated wind disturbance coincides with the actual wind velocity.

The following section provides a quantitative performance comparison for the proposed path prediction methods, as well as an assessment of wind estimation accuracy for the pose-plus-wind prediction method.

4.1. Prediction performance

In Section 2.3, e_k^{p} is defined as an averaged distance error between the predicted position history and the actual position history at time step k. The averaged e_k^{p} during a flight is defined as e_{p}, and this is used to evaluate the prediction performance in this section. As indicated in Table 1, the entire paths of the eSPAARO and Bixler are segmented to 3 types of flight, and the prediction performance is evaluated for each type of flight.

The measurements of the threat aircraft position and attitude are assumed to be available from an on-board sUAS sensing system of the host aircraft. In practice, this sensing system might be a vision-based system as described in [33]. However, fixed-wing flight imagery that is amenable to the analysis described here, together with the independent motion data that are needed for validation, is currently unavailable to the authors. (A flight campaign is planned to address this data shortage.) The flight data used to assess performance of the algorithms described here were therefore obtained directly from the Pixhawk 1 autopilot data recorded by each threat aircraft. As a result, the flight data used here are likely much more accurate than observations from the on-board sUAS sensing system. Our interest here, however, is in comparing the relative performance of three distinct approaches, rather than assessing the absolute performance using a particular measurement system. Having said that, we certainly have an interest in how path prediction performance might vary as a result of noise in the observations. Reference [43] describes the performance of a ground-based radar for detecting and tracking a sUAS (a DJI Phantom 2), citing a range accuracy better than 2 m. By comparison, a small, on-board radar described in [53] provides a position estimation accuracy on the order of 5 m. To simulate measurement uncertainty in the envisioned scenario, we superimpose zero-mean Gaussian noise, with a 5 m standard deviation, on the threat position. Similarly, we add zero-mean Gaussian noise to the threat attitude angles; the standard deviation is based on measurements from the vision-based pose estimation strategy reported in [33] and summarized in Table 3. We apply a Kalman filter to the artificially noise-corrupted measurement data and then apply the prediction algorithms to these filtered data as described.

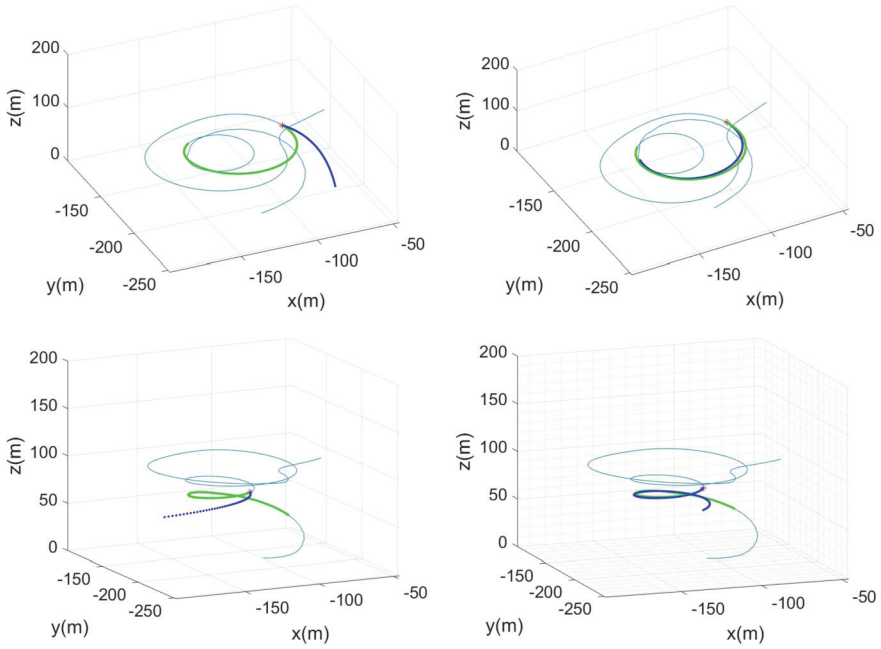

Fig. 3. Path prediction (blue line) using position data only (left column) and pose-plus-wind (right column). The top and bottom plots show predictions at different times within the same data set, and from different view points. (For interpretation of the colors in the figure(s), the reader is referred to the web version of this article.)

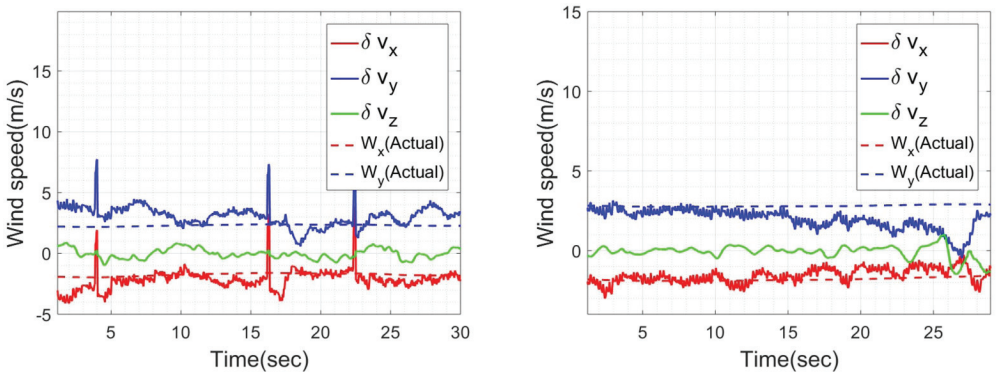

Fig. 4. Wind estimation for the eSPAARO over two 30-second intervals.

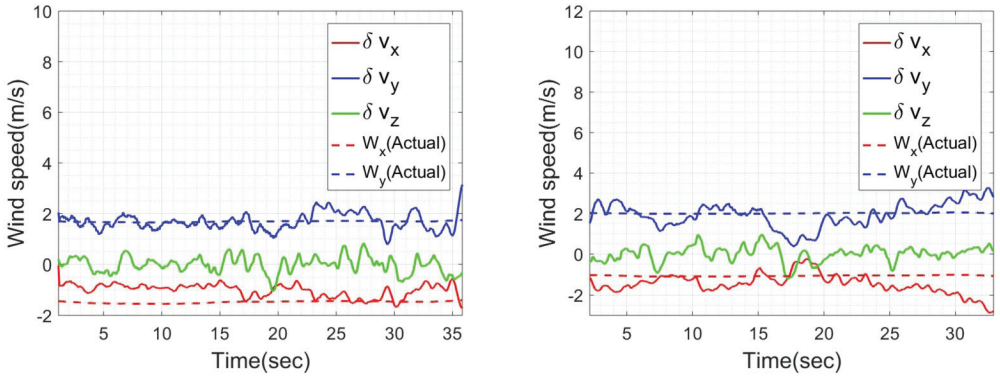

Fig. 5. Wind estimation for the Bixler over two 30-second intervals.

Figs. 6, 8 and 10 show e_p computed based on uncorrupted telemetry data; Figs. 7, 9 and 11 show e_p with artificial noise superimposed on the telemetry data. For these bar graphs, the index for the given path segment appears on the x-axis; the height of the bars represents the prediction error e_p. Black bars show e_p for position-based prediction, white bars show e_p for pose-based prediction (i.e., based on position and attitude), and gray bars show e_p for pose-plus-wind prediction.

In Fig. 6, which pertains to straight flight path segments, the position-based prediction method generally outperforms pose-based prediction for the eSPAARO (left) and the Bixler (right). Pose-plus-wind prediction generally outperforms both of these other

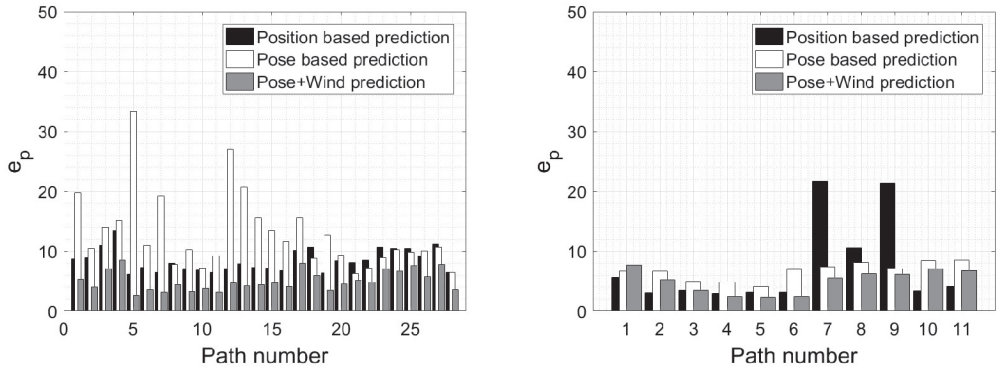

Fig. 6. Averaged distance error e_p for straight flight of two aircraft without noise (left: eSPAARO, right: Bixler).

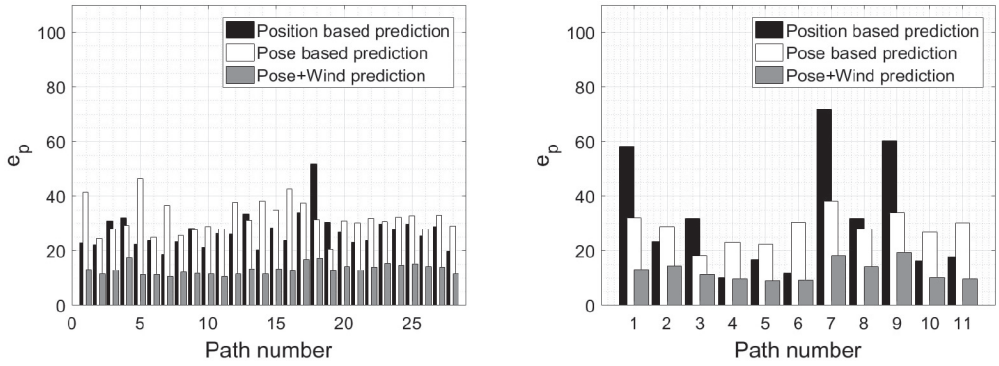

Fig. 7. Averaged distance error e_p for straight flight of two aircraft with noisy data (left: eSPAARO, right: Bixler).

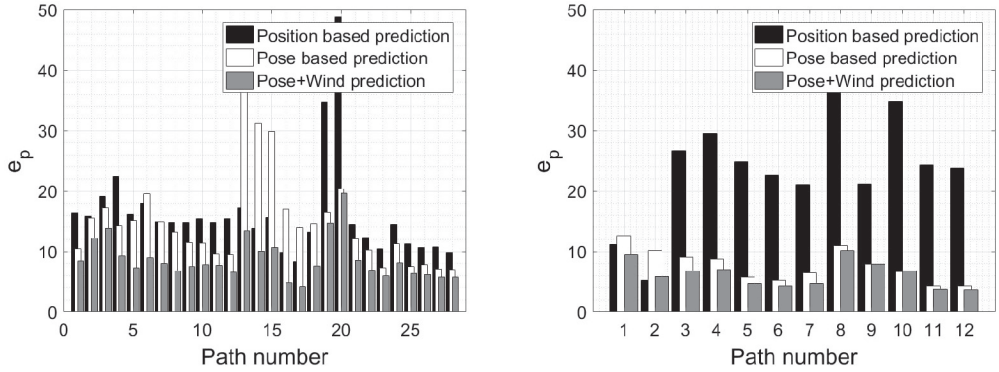

Fig. 8. Averaged distance error e_p for turning flight of two aircraft without noise (left: eSPAARO, right: Bixler).

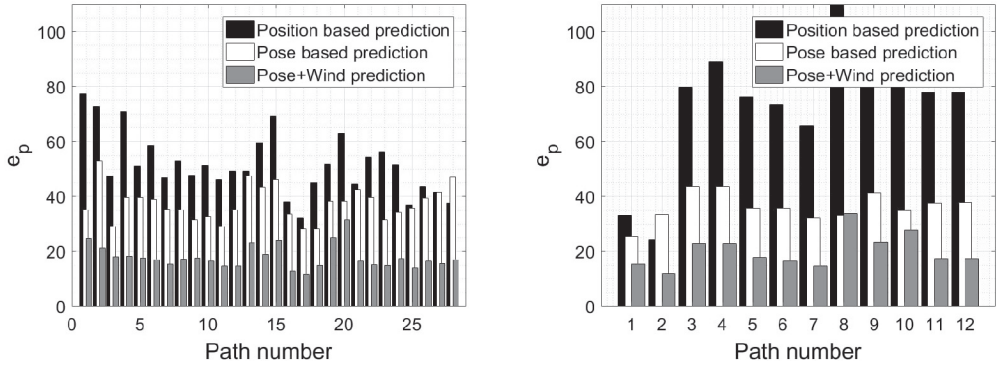

Fig. 9. Averaged distance error e_p for turning flight of two aircraft with noisy data (left: eSPAARO, right: Bixler).

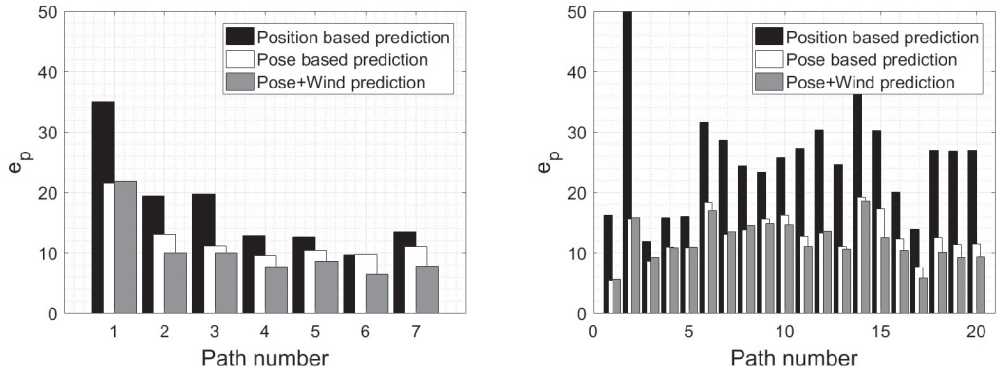

Fig. 10. Averaged distance error e_p for maneuvering flight of two aircraft without noise (left: eSPAARO, right: Bixler).

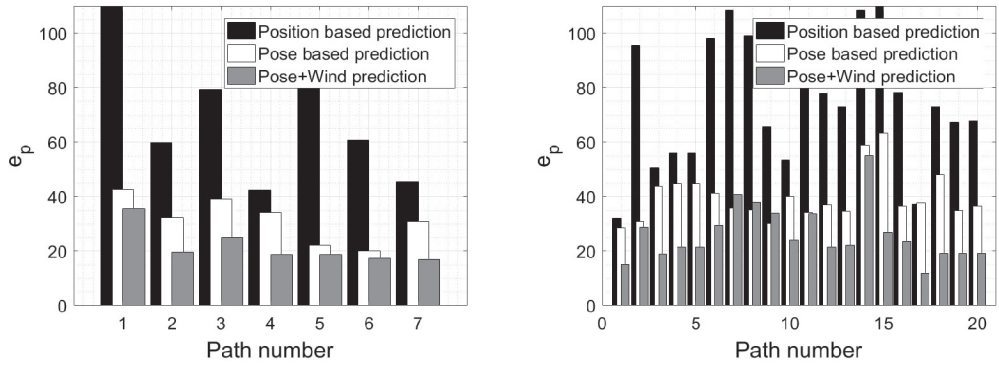

Fig. 11. Averaged distance error e_p for maneuvering flight of two aircraft with noisy data (left: eSPAARO, right: Bixler).

Table 3
Average error magnitude for pose estimation experiments described in [33].

Value	Roll	Pitch	Yaw
Average error magnitude (°)	3.4	2.7	11.6

methods for both aircraft. When artificial noise is introduced, the pose-based algorithm performs worse than position-based prediction for both aircraft, as seen in Fig. 7. Note that pose-based prediction will be in error if the aircraft does not point in the direction it is traveling. This happens, for example, when the aircraft "crabs" into an ambient wind in order to maintain a commanded course.

For turning flight (Figs. 8 and 9), pose-based prediction generally outperforms position-based prediction for the Bixler, with or without noise, and also for the eSPAARO when artificial noise is injected into the measurements.

For maneuvering flight (Figs. 10 and 11), the results generally match those for turning flight. The pose-plus-wind approach does not provide such a dramatic improvement as in the earlier cases, but this approach still consistently outperforms the alternatives.

4.2. Wind estimation

As stated in Section 2.3, the wind disturbance $\delta\vec{\boldsymbol{v}}$ is estimated to correct the path prediction. Here, the estimated wind disturbance is compared with the "true" wind velocity, that is, the wind velocity estimated by the Pixhawk 1 autopilot's integrated wind estimation scheme. Figs. 12, 14 and 16 show the averaged wind estimation error based on the pose-plus-wind algorithm applied directly to telemetry data. Figs. 13, 15 and 17 show the wind estimation error when artificial noise is injected into the measurements. Black and gray bars indicate the magnitude of the wind estimation error, $|\delta v_x - W_x|$ and $|\delta v_y - W_y|$, respectively. For most cases involving the Bixler, the wind estimation error is quite low compared with that for the eSPAARO aircraft. We conjecture that because the Bixler is smaller, lighter, and slower than the eSPAARO, it is more susceptible to wind disturbances, making estimation of these wind disturbances easier. The wind estimates predictably degrade with the injection of artificial noise. The results suggest that the wind velocity in the vicinity of a small unmanned aircraft can be estimated using the algorithm suggested here, provided the wind disturbances have a visible influence on aircraft motion and the measurement error is low. Alternatively, if the host aircraft is capable of measuring the wind in its own vicinity, it may be reasonable over short distances to assume this wind field is constant and uniform so that the same wind affects the threat aircraft. In general, though, the ability to infer the wind disturbance acting on a distant aircraft can be useful in predicting its path.

5. Conclusion

Three methods to predict the path of a fixed-wing aircraft were proposed and compared. These methods all assume that the aircraft position can be inferred, for example, from a sUAS sensing system. In addition, a vision system may provide the attitude of the observed aircraft which can be used, together with a particle dynamic model for aircraft flight, to predict the path. Moreover, one may obtain even more accurate predictions by using measurement residuals to infer the ambient wind in the vicinity of the threat. To demonstrate and assess the performance of the proposed algorithms, experimental flight data for two small fixed-wing unmanned aircraft were used. The results show that position- and pose-based prediction perform comparably for straight flight while pose-based prediction generally outperforms position-based prediction for turning or maneuvering flight. Pose-plus-wind prediction, in which measurements of the aircraft position and attitude

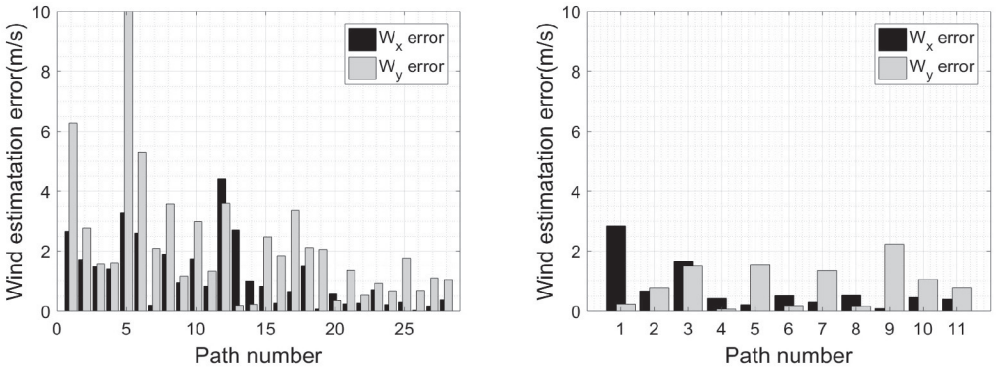

Fig. 12. Wind estimation error of straight flight from two aircraft without noise (left: eSPAARO, right: Bixler).

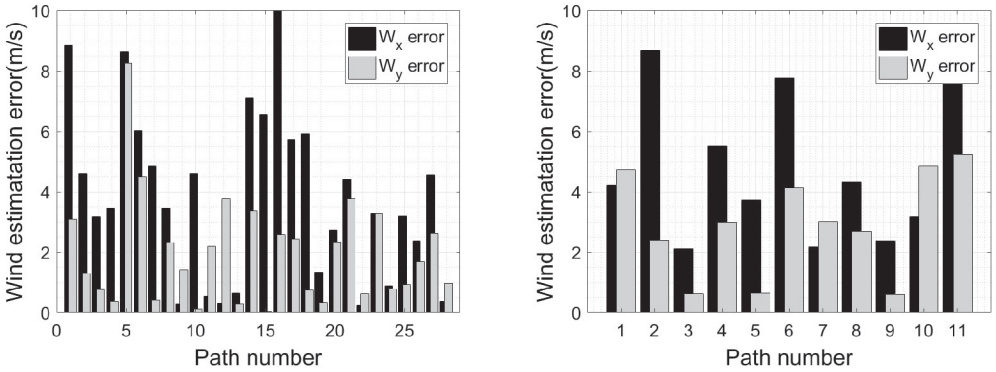

Fig. 13. Wind estimation error of straight flight from two aircraft with artificial noise (left: eSPAARO, right: Bixler).

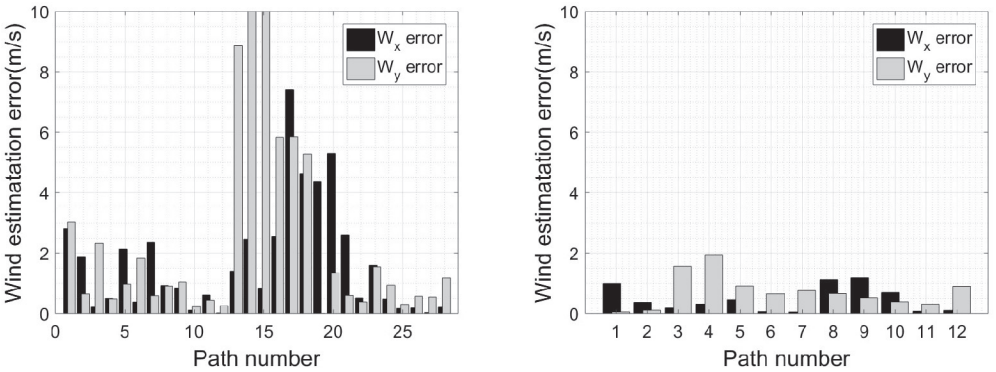

Fig. 14. Wind estimation error of turning flight from two aircraft without noise (left: eSPAARO, right: Bixler).

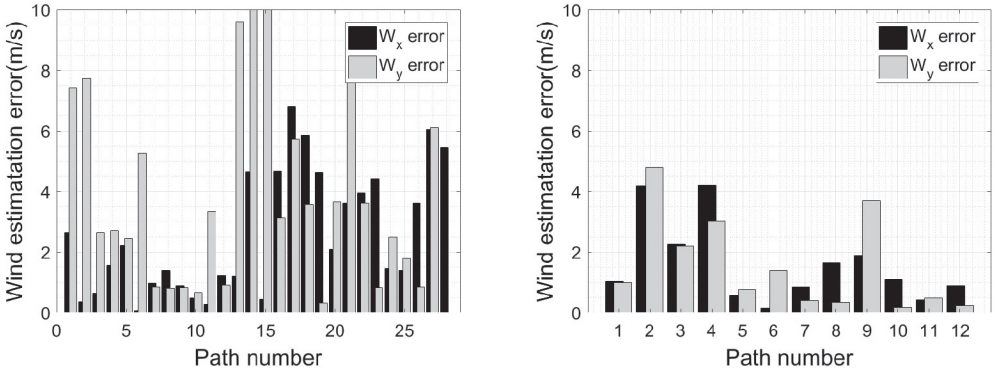

Fig. 15. Wind estimation error of turning flight from two aircraft with artificial noise (left: eSPAARO, right: Bixler).

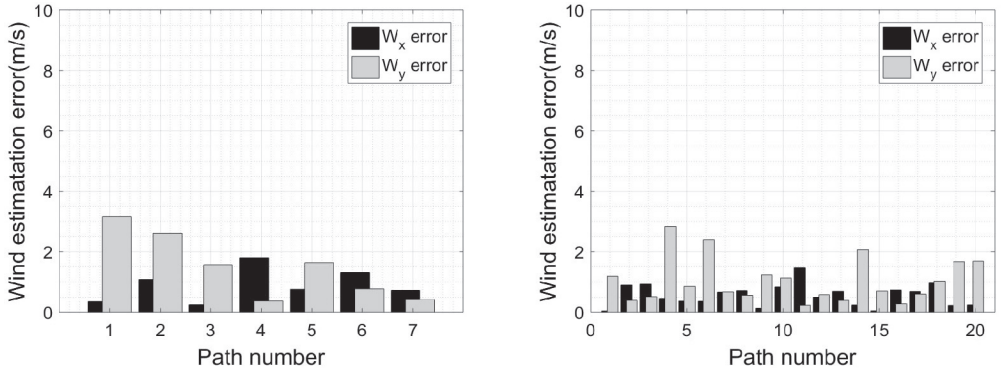

Fig. 16. Wind estimation error of maneuvering flight from two aircraft without noise (left: eSPAARO, right: Bixler).

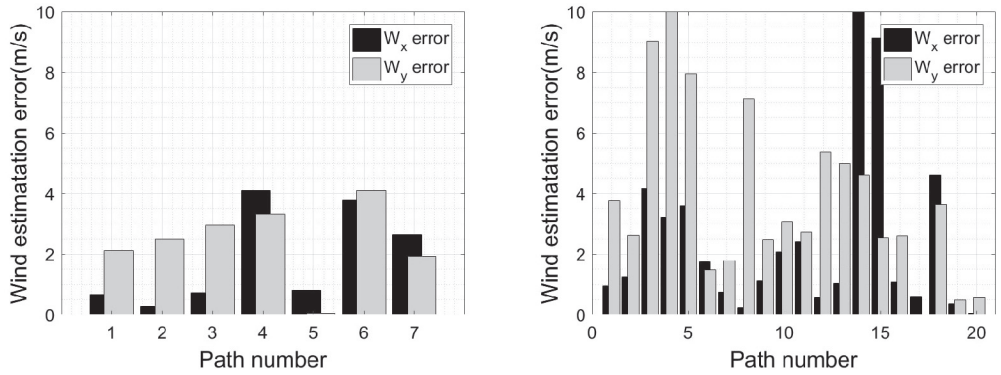

Fig. 17. Wind estimation error of maneuvering flight from two aircraft with artificial noise (left: eSPAARO, right: Bixler).

are used along with estimates of the wind velocity, shows the best performance among these three approaches for all of types of flight and both types of aircraft. Comparisons of the estimated wind disturbance and the actual wind velocity show that the wind estimation error for the smaller, lighter aircraft is quite small relative to the wind estimation error for the larger, faster aircraft. For the smaller aircraft, a given wind disturbance has a greater effect on position and attitude, which are estimated for use in the prediction algorithm. Ongoing efforts aim to develop the path prediction algorithm for other types of aircraft, such as multi-rotor aircraft, and to implement the algorithm for real-time operation in experimental hardware.

Declaration of competing interest

The authors declare that they have no known competing financial interests or personal relationships that could have appeared to influence the work reported in this paper.

Acknowledgements

The authors gratefully acknowledge the support of the Center for Unmanned Aircraft Systems, a National Science Foundation (NSF) Industry/University Cooperative Research Center (I/UCRC) under NSF Grant No. CNS-1650465.

References

[1] B. Mueller, A. Tsang, At a busy airport in Britain, only pesky drones are flying, N.Y. Times (2018) A1.
[2] C.E. Lin, Y.H. Lai, UAV path prediction for CD&R to manned aircraft in a confined airspace for cooperative mission, Int. J. Aerosp. Eng. 2018 (1) (2018) 1–9, https://doi.org/10.1155/2018/8759836.
[3] J.K. Kuchar, L.C. Yang, A review of conflict detection and resolution modeling methods, IEEE Trans. Intell. Transp. Syst. 1 (4) (2000) 179–189, https://doi.org/10.1109/6979.898217.
[4] X. Olive, J. Morio, Trajectory clustering of air traffic flows around airports, Aerosp. Sci. Technol. 84 (2019) 776–781, https://doi.org/10.1016/j.ast.2018.11.031.
[5] P. Pierpaoli, A. Rahmani, UAV collision avoidance exploitation for noncooperative trajectory modification, Aerosp. Sci. Technol. 73 (2018) 173–183, https://doi.org/10.1016/j.ast.2017.12.008.
[6] Y. Lin, S. Saripalli, Path planning using 3D Dubins curve for unmanned aerial vehicles, in: 2014 International Conference on Unmanned Aircraft Systems (ICUAS), Orlando, Florida, May 27–30, 2014, pp. 296–304.
[7] M. Laurenzis, M. Rebert, S. Schertzer, F. Christnacher, Tracking and prediction of small unmanned aerial vehicles' flight behavior and three-dimensional flight path, in: SPIE Defense + Commercial Sensing, Baltimore, Maryland, April 16–18, 2019.
[8] A.C. Canolla, M.B. Jamoom, B. Pervan, Unmanned aircraft systems detect and avoid sensor hybrid estimation error analysis, in: 17th AIAA Aviation Technology, Integration, and Operations Conference, Denver, Colorado, June 5–9, 2017, p. 4384.
[9] S.T. Kanneganti, P.B. Chilson, R. Huck, Visualization and prediction of aircraft trajectory using ADS-B, in: Dayton, Ohio July 23–26, 2018, pp. 529–532.
[10] Y. Lin, S. Saripalli, Sampling-based path planning for UAV collision avoidance, IEEE Trans. Intell. Transp. Syst. 18 (11) (2017) 3179–3192, https://doi.org/10.1109/TITS.2017.2673778.
[11] M. Hammer, M. Hebel, M. Laurenzis, M. Arens, Lidar-based detection and tracking of small UAVs, in: Emerging Imaging and Sensing Technologies for Security and Defence III; and Unmanned Sensors, Systems, and Countermeasures, Berlin, Germany, September 10–13, 2018.
[12] Z. Wu, J. Li, J. Zuo, S. Li, Path planning of UAVs based on collision probability and Kalman filter, IEEE Access 6 (2018) 34237–34245, https://doi.org/10.1109/ACCESS.2018.2817648.
[13] C. Sakthivel, B. Sureshkumar, R. Ramkumar, R. Yokeswaran, Detection and path prediction of aircraft based on acoustics and vibration, Mater. Today, Proc. 21 (2020) 588–591, https://doi.org/10.1016/j.matpr.2019.06.720.
[14] X. Zhang, C. Fan, J. Fang, S. Xu, J. Du, Tracking prediction to avoid obstacle path of agricultural unmanned aerial vehicle based on particle filter, Proc. Inst. Mech. Eng., Part I, J. Syst. Control Eng. 232 (4) (2018) 408–416, https://doi.org/10.1177/0959651817710128.
[15] Y. Lin, S. Saripalli, Collision avoidance for UAVs using reachable sets, in: 2015 International Conference on Unmanned Aircraft Systems (ICUAS), Denver, Colorado, June 9–12, 2015, pp. 226–235.
[16] L. Ren, M. Castillo-Effen, H. Yu, Y. Yoon, T. Nakamura, E.N. Johnson, C.A. Ippolito, Small unmanned aircraft system (sUAS) trajectory modeling in support of UAS

traffic management (UTM), in: 17th AIAA Aviation Technology, Integration, and Operations Conference, Denver, Colorado, June 5–9, 2017.
[17] R. Slattery, Y. Zhao, Trajectory synthesis for air traffic automation, J. Guid. Control Dyn. 20 (2) (1997) 232–238, https://doi.org/10.2514/2.4056.
[18] S. Vilardaga, X. Prats, Mass estimation for an adaptive trajectory predictor using optimal control, in: Proceedings of the 5th International Conference on Application and Theory of Automation in Command and Control Systems, Toulouse, France, September 30–October 2, 2015, pp. 75–84.
[19] W. Glover, J. Lygeros, A multi-aircraft model for conflict detection and resolution algorithm evaluation, in: Technical Report WP1, Deliverable D1.3, Version 1.3, HYBRIDGE, 2003.
[20] S. Ayhan, H. Samet, Aircraft trajectory prediction made easy with predictive analytics, in: Proceedings of the 22nd ACM SIGKDD International Conference on Knowledge Discovery and Data Mining, San Francisco, California, August 13–17, 2016, pp. 21–30.
[21] I. Lymperopoulos, J. Lygeros, A. Lecchini, Model based aircraft trajectory prediction during takeoff, in: AIAA Guidance, Navigation, and Control Conference and Exhibit, Keystone, Colorado, August 21–24, 2006.
[22] J. Zhang, J. Liu, R. Hu, H. Zhu, Online four dimensional trajectory prediction method based on aircraft intent updating, Aerosp. Sci. Technol. 77 (2018) 774–787, https://doi.org/10.1016/j.ast.2018.03.037.
[23] W. Chan, R. Bach, J. Walton, Improving and validating ctas performance models, in: AIAA Guidance, Navigation, and Control Conference and Exhibit, Denver, Colorado, August 14–17, 2000.
[24] A.W. Warren, Y.S. Ebrahimi, Vertical path trajectory prediction for next generation ATM, in: Proceedings of the 17th DASC, AIAA/IEEE/SAE, Digital Avionics Systems Conference, Bellevue, Washington, October 31–November 7, vol. 2, 1998, pp. F11/1–F11/8.
[25] A. Hadjaz, G. Marceau, P. Savéant, M. Schoenauer, Online learning for ground trajectory prediction, preprint, arXiv:1212.3998, 2012.
[26] H.T. Lee, G. Chatterji, Closed-form takeoff weight estimation model for air transportation simulation, in: 10th AIAA Aviation Technology, Integration, and Operations, (ATIO) Conference, Fort Worth, Texas, September 13–15, 2010.
[27] M. Lopez-Lago, R. Casado, A. Bermudez, J. Serna, A predictive model for risk assessment on imminent bird strikes on airport areas, Aerosp. Sci. Technol. 62 (2017) 19–30, https://doi.org/10.1016/j.ast.2016.11.020.
[28] R. Alligier, D. Gianazza, N. Durand, Machine learning and mass estimation methods for ground-based aircraft climb prediction, IEEE Trans. Intell. Transp. Syst. 16 (6) (2015) 3138–3149, https://doi.org/10.1109/TITS.2015.2437452.
[29] D.P. Thipphavong, C.A. Schultz, A.G. Lee, S.H. Chan, Adaptive algorithm to improve trajectory prediction accuracy of climbing aircraft, J. Guid. Control Dyn. 36 (1) (2012) 15–24, https://doi.org/10.2514/1.58508.
[30] G.L. Slater, Adaptive improvement of aircraft climb performance for air traffic control applications, in: Proceedings of the IEEE International Symposium on Intelligent Control, Vancouver, Canada, Oct 30, 2002, pp. 602–607.
[31] A.A. Godbole, Adaptive Improvement of Climb Performance, Master's thesis, University of Cincinnati, 2003, Retrieved from https://etd.ohiolink.edu/pg_10?0::NO:10:P10_ACCESSION_NUM:ucin1061303791.
[32] A. Nuic, User Manual for the Base of Aircraft Data (BADA) Revision 3.10, ATMosphere, 2010.
[33] C. Kang, J. Davis, C.A. Woolsey, S. Choi, Sense and avoid based on visual pose estimation for small UAS, in: 2017 IEEE/RSJ International Conference on Intelligent Robots and Systems (IROS), Vancouver, Canada, September 24–28, 2017, pp. 3473–3478.
[34] C. Kang, H. Chaudhry, C.A. Woolsey, K.B. Kochersberger, Development of a peripheral-central vision system for small UAS tracking, in: AIAA SciTech, San Diego, California, January 7–11, 2019.
[35] C.M. Lin, C.Y. Tsai, Y.C. Lai, S.A. Li, C.C. Wong, Visual object recognition and pose estimation based on a deep semantic segmentation network, IEEE Sens. J. 18 (22) (2018) 9370–9381, https://doi.org/10.1109/JSEN.2018.2870957.
[36] Y. Wang, X. Tan, Y. Yang, X. Liu, E. Ding, F. Zhou, L.S. Davis, 3D pose estimation for fine-grained object categories, in: European Conference on Computer Vision (ECCV), Munich, Germany, September 8–14, 2018.
[37] P. Poirson, P. Ammirato, C.Y. Fu, W. Liu, J. Kosecka, A.C. Berg, Fast single shot detection and pose estimation, in: 2016 Fourth International Conference on 3D Vision (3DV), Stanford, California, October 25–28, 2016, pp. 676–684.
[38] G. Billings, M. Johnson-Roberson, Silhonet: an rgb method for 3D object pose estimation and grasp planning, preprint, arXiv:1809.06893, 2018.
[39] Y. Xiang, W. Kim, W. Chen, J. Ji, C. Choy, H. Su, R. Mottaghi, L. Guibas, S. Savarese, Objectnet3D: a large scale database for 3D object recognition, in: European Conference on Computer Vision (ECCV), Amsterdam, Netherlands, October 11–14, 2016, pp. 160–176.
[40] P. Wellig, P. Speirs, C. Schuepbach, R. Oechslin, M. Renker, U. Boeniger, H. Pratisto, Radar systems and challenges for C-UAV, in: 2018 19th International Radar Symposium (IRS), Bonn, Germany, June 20–22, 2018, pp. 1–8.
[41] M.E. Rovkin, V.A. Khlusov, N.D. Malyutin, A.V. Hristenko, A.S. Novikov, D.M. Nosov, M.V. Osipov, M.O. Konovalenko, A.O. Marchenko, V.E. Ilchenkoy, Radar detection of small-size UAVs, in: 2018 Ural Symposium on Biomedical Engineering, Radioelectronics and Information Technology (USBEREIT), Yekaterinburg, Russia, May 7–8, 2018, pp. 371–374.
[42] S. Samaras, E. Diamantidou, D. Ataloglou, N. Sakellariou, A. Vafeiadis, V. Magoulianitis, A. Lalas, A. Dimou, D. Zarpalas, K. Votis, P. Daras, Deep learning on multi sensor data for counter UAV applications—a systematic review, Sensors 19 (22) (2019) 4837, https://doi.org/10.3390/s19224837.
[43] P. Poitevin, M. Pelletier, P. Lamontagne, Challenges in detecting UAS with radar, in: 2017 International Carnahan Conference on Security Technology (ICCST), Madrid, Spain, October 23–26, 2017, pp. 1–6.
[44] A.C. Canolla, M.B. Jamoom, B. Pervan, Unmanned aircraft systems detect and avoid sensor hybrid estimation error analysis, in: 17th AIAA Aviation Technology, Integration, and Operations Conference, Denver, Colorado, June 5–9, 2017.
[45] J. Anderson, Introduction to Flight, 3rd edition, McGraw-Hill, New York City, New York, 2008.
[46] N.X. Vinh, Flight Mechanics of High-Performance Aircraft, Vol. 4, Cambridge University Press, Cambridge, United Kingdom, 1995.
[47] L.R. Sahawneh, R.W. Beard, Path planning in the local-level frame for small unmanned aircraft systems, in: Kinematics, IntechOpen, 2017.
[48] X.R. Li, V.P. Jilkov, Survey of maneuvering target tracking. Part I. Dynamic models, IEEE Trans. Aerosp. Electron. Syst. 39 (4) (2003) 1333–1364, https://doi.org/10.1109/TAES.2003.1261132.
[49] U. Maeder, M. Morari, T.I. Baumgartner, Trajectory prediction for light aircraft, J. Guid. Control Dyn. 34 (4) (2011) 1112–1119, https://doi.org/10.2514/1.52124.
[50] R. Alligier, D. Gianazza, M.G. Hamed, N. Durand, Comparison of two ground-based mass estimation methods on real data, in: ICRAT 2014, 6th International Conference on Research in Air Transportation, Istanbul, Turkey, May 26–30, 2014.
[51] R. Alligier, D. Gianazza, N. Durand, Energy rate prediction using an equivalent thrust setting profile, in: ICRAT 2012, 5th International Conference on Research in Air Transportation, Berkeley, California, May 22–25, 2012.
[52] C. Schultz, D. Thipphavong, H. Erzberger, Adaptive trajectory prediction algorithm for climbing flights, in: AIAA Guidance, Navigation, and Control Conference, Minneapolis, Minnesota, August 13–16, 2012.
[53] H.G. McClelland, C. Kang, C.A. Woolsey, A.K. Roberts, D. Buck, T. Cheney, K. Warnick, Small aircraft flight encounters database for UAS sense and avoid, in: AIAA SciTech, Grapevine, Texas, January 9–13, 2017.